

Please cite the Published Version

Shi, X, Shi, Y, Chen, J, Liskiewicz, TW, Beake, BD, Zhou, Z, Wang, Z and Wu, G (2021) Influence of gradient interlayer thickness on corrosion and tribological behavior of Ti-containing multilayer graphite-like carbon films. *Wear*, 488-48. ISSN 0043-1648

DOI: <https://doi.org/10.1016/j.wear.2021.204177>

Publisher: Elsevier

Version: Accepted Version

Downloaded from: <https://e-space.mmu.ac.uk/628761/>

Usage rights: © In Copyright

Additional Information: This is an Author Accepted Manuscript of an article published in *Wear*.

Enquiries:

If you have questions about this document, contact openresearch@mmu.ac.uk. Please include the URL of the record in e-space. If you believe that your, or a third party's rights have been compromised through this document please see our Take Down policy (available from <https://www.mmu.ac.uk/library/using-the-library/policies-and-guidelines>)

Influence of gradient interlayer thickness on corrosion and tribological behavior of Ti-containing multilayer graphite-like carbon films

Xiangru Shi^{a*}, Yunjia Shi^a, Jian Chen^b, Tomasz W. Liskiewicz^c, Ben D. Beake^d,
Zehua Zhou^a, Zehua Wang^a, Guosong Wu^a

a. College of Mechanics and Materials, Hohai University, Nanjing 210098, China

b. School of Materials Science and Engineering, Jiangsu Key Laboratory for Advanced Metallic Materials, Southeast University, Nanjing 211189, China

c. Faculty of Science and Engineering, Manchester Metropolitan University, John Dalton Building, Charles Street, Manchester M15 6BH, UK

d. Micro Materials Ltd., Willow House, Yale Business Village, Ellice Way, Wrexham, LL13 7YL, UK

* Corresponding author. E-mail address: sxr12009210@163.com

Abstract

Structural design is a crucial strategy to improve the service performance of amorphous carbon films in aggressive environments. In this study multilayered graphite-like carbon (GLC) films with adhesive layer/gradient interlayer/doping layer architectures with varied gradient interlayer thickness were deposited on 316L stainless steel substrates by closed field unbalanced magnetron sputtering. The effect of gradient interlayer thickness on microstructure, mechanical, tribological and corrosion behavior of the GLC films was investigated. The results show that the mechanical properties and bonding strength decrease with increasing gradient interlayer thickness due to the increased sp^2 content, surface roughness and decreased film integrity. The friction coefficient curves in ambient air and 3.5% NaCl solution show similar three-stage feature with distinctive wear mechanism in stage III. The decreased mechanical properties and loose microstructure of GLC films with thicker gradient interlayer thickness caused the decreased wear resistance in both ambient air and NaCl solution. In comparison with the uncoated substrate, the GLC films show improved corrosion resistance in NaCl solution, which also decreases with the increased gradient interlayer thickness due to the low film compactness and high electrical conductivity.

Keywords: graphite-like carbon films, gradient interlayer, tribological performance, corrosion resistance, wear mechanism

1. Introduction

Due to their good processability, high mechanical strength and excellent corrosion resistance, stainless steels have been widely used in petroleum, chemical, metallurgical, mining, biomedical, marine and other industrial fields [1,2]. However, some stainless steel components, such as valves, bearings, propellers, pumps and sealing rings operating in aggressive environments, not only have to resist corrosion damage, but also often are subject to mechanical wear, resulting in rapid failure of mechanical parts and unnecessary economic losses [3-5]. Therefore, it's of considerable industrial importance to develop and study high-performance wear-resistant and corrosion-resistant coating materials to protect the components, and to explore the corrosion, wear behavior and failure mechanisms under harsh conditions.

As solid self-lubricating materials, amorphous carbon films (a-C), consisting of mainly sp^2 and sp^3 hybridized carbon atoms, have been considered as promising candidates for improving the safety, stability and durability of metallic components simultaneously under corrosion and friction conditions [6-9]. In terms of the relative amount of sp^2 and sp^3 hybrid bonds in the film structure, a-C can be divided into diamond-like carbon (DLC, sp^3 dominate) and graphite-like carbon (GLC, sp^2 dominate) [10-12]. In contrast to many other DLC films, GLC films have demonstrated superior tribological properties in water or other humid environments, due to their high hardness, low friction coefficient, high wear resistance, corrosion resistance and high chemical stability [12-15]. For example, Wang et al. [14,15] compared the friction and wear behavior of GLC films in ambient air and water against different metallic and ceramic counterparts. It was found that almost all the friction coefficients and wear rates of GLC films were lower in water than in ambient air, except for coupling with the ZrO_2 ceramic ball, which was attributed to partial water fluid lubrication and the reduction of adhesion or abrasion between the GLC films and various counterparts in water. Recently, Yan et al. [13] systematically investigated the tribological properties of Cr-GLC and Cr-DLC under a dry condition and two ionic liquids using a ball-on-disc tribometer. They found there was an approximately 40% reduction of friction coefficient in ionic liquids compared to that under dry condition. In addition, the compact microstructure and the formation of a physicochemical tribofilm promoted better friction and wear behavior of Cr-DLC than the Cr-GLC. Nevertheless, the tribological properties of GLC films in corrosion solution are still far less understood than that of DLC films, and the wear mechanism in corrosion solution is not clear. In particular, there is almost no research on the corrosion resistance of GLC films.

Alongside this, a major challenge to maintain the long-term stability of GLC films in

the harsh environments is to solve the problems of high residual stress, low adhesion strength and abundant surface defects of the films [16-19]. The corrosion medium can destroy the interface between the film and the substrate through the pores and defects in the film, leading to catastrophic failure of the components. One common strategy is to add an interlayer between the film and substrate, which can mitigate the performance difference between the film and the substrate, and extend the diffusion path of corrosive media, leading to improvement of the corrosion and wear resistance of the films [10,20-22]. Although different interlayers can make different positive contributions to the performance of GLC films, the gradient interlayer was reported as the optimal solution since the gradient distribution of the Me/C (Me refers to metallic elements such as Cr [10], Ti [23], Al [24] or W [25]) composition eliminates the abrupt chemical or mechanical changes in the film/substrate interface. Wang et al. [25] suggested that the gradient Cr/C interlayer in the GLC film contribute to higher hardness, improved adhesion strength and load-bearing capacity, while the GLC films with single Cr interlayer and thickness gradient Cr/C interlayer show only a small improvement in mechanical properties. Zhu et al. [26] showed that the gradient CrC and CrNC interlayer provided better corrosion resistance for hydrogenated DLC films than the constant CrC interlayer in Hank's solution. Moreover, it is noteworthy that a suitable thickness of the interlayer is vital to the properties of a-C films. Shahsavari et al. [27] reported that the DLC film with 20 nm Cr interlayer exhibited the best hardness and wear resistance due to the lowest surface roughness and the optimal distribution of Cr particles on the substrate. Chen et al. [28] studied the effect of SiN_x interlayer thickness on the microstructure, adhesion and tribological properties of DLC films. It was found that the surface roughness and internal stress decreased first and then increased with the increase of the SiN_x interlayer thickness, while the film with interlayer thickness of 10 nm had the best tribological and mechanical properties, resulting from the aggregation of nitrogen vacancy center. Hincapie C et al. [29] revealed that the Ti_xSi interlayer with 200 nm thickness improved the critical load capacity between the DLC film and 316L stainless steel, while complete delamination was observed for interlayers with other thickness at the same loading conditions. However, to the best knowledge of the authors, little attention was paid to the effect of gradient interlayer thickness on the microstructure, adhesion strength, mechanical properties, wear and especially corrosion resistance of GLC films.

In the present work, the multilayer Ti-GLC films with different Ti-C gradient interlayer thickness were deposited on 316L stainless steel by unbalanced magnetron sputtering. The microstructure, composition, adhesion strength and mechanical properties were comparatively investigated as a function of gradient interlayer thickness. The purpose

of this paper is mainly to explore a solution to the long-term and extensive application of GLC films under aggressive environments and to fill up the research gap on the effect of gradient interlayer thickness on the properties of GLC films.

2. Experimental

2.1. Film preparation

GLC films were deposited on Si (100) wafer and mirror-polished 316L stainless steel substrates (20×20×0.5 mm) by closed field unbalanced magnetron sputtering system (UDP-650/4, Teer Coating Ltd., UK). Two graphite targets (purity 99.99%) and two Ti targets (purity 99.99%) were symmetrically positioned in the cylindrical chamber with a three-axis substrate rotation worktable to prepare uniform films. Before deposition, the substrates were cleaned ultrasonically in deionized water, ethanol and acetone for 20 min, respectively, and then fixed in the vacuum chamber with a base pressure below 3.0×10^{-5} Pa. Subsequently, the substrates underwent further Ar^+ bombardment at a bias voltage of -500 V for 30 min to remove the surface oxide contamination, following target-cleaning at -120 V bias voltage for 5 min. Then, a Ti bottom layer was produced on the substrate surfaces at 3 A Ti target current and -60 V bias voltage for 15 min. Afterward, the gradient Ti-C layers with different thickness were deposited by decreasing Ti target current to 0.8 A and simultaneously increasing graphite target current to 3 A over 15 min, 30 min, and 60 min, respectively. Finally, uniform Ti-containing GLC function layer was prepared by maintaining the deposition parameters of the previous step for 60 min. The detailed preparation parameters have been listed in Table 1. For simplicity, multilayer Ti-GLC films with different gradient layer thickness will be referred to hereafter as GLC-1, GLC-2 and GLC-3.

Table 1. Deposition parameters for GLC films with different gradient interlayer thickness.

Process	Substrate clean	Target clean	Adhesive layer	Gradient interlayer	Doping GLC layer
				15 (GLC-1)	
Time (min)	30	5	15	30 (GLC-2)	60
				60 (GLC-3)	
Substrate bias (V)	-500	-120	-60	-60	-60
Ti target current (A)	0.5	2	3	3-0.8	0.8
C target current (A)	0	0	0.3	0.3-3	3

2.2 General characterization

The microstructure and composition of the as-deposited GLC films were characterized by using the coated Si substrates. Surface and cross-sectional morphologies of the films were examined by scanning electron microscopy (SEM, XL-30, FEI Co., USA) at 20.0 KV. The composition evolution of the multilayer GLC films was detected from the cross-sectional morphologies with the attached EDX spectrum. The film thickness was also measured from the cross-sectional SEM images. The three-dimensional surface topographies and R_a surface roughness measurements were determined by atomic force microscopy (AFM, Bruker Co., Germany) at a scanning speed of 1 Hz and a test area of $1 \times 1 \mu\text{m}^2$. X-ray diffraction (XRD, D8-Discover, Bruker Co., German) in the 2θ range of $10\text{-}30^\circ$ was carried out to investigate the amorphous structure of the as-deposited films. Raman spectroscopy (Alpha300R, WITec Co., Germany) was used to characterize the carbon atom bonds by using an Ar^+ laser of 532 nm in the spectra range of $1000\text{-}2000 \text{ cm}^{-1}$. X-ray photoelectron spectroscopy (XPS, Thermo Scientific K-Alpha, ThermoFisher Co., USA) was performed to analyze the bonding state and chemical composition of the GLC films with monochromatic $\text{AlK}\alpha$ irradiation.

2.3 Mechanical testing

Hardness (H) and elastic modulus (E) of the as-deposited GLC films were evaluated by a calibrated nanoindentation system (NanoTest Vantage, Micro Materials Ltd., UK) with a Berkovich diamond indenter. The maximum indentation depth was set to no more than 10% of the film thickness to minimise the influence of the underlying substrate on the results, and fifteen repeated tests were conducted on each sample to

mitigate the effect of surface roughness and defects in the films. The data was analyzed according to Oliver and Pharr's method. The scratch adhesion of the films was investigated by a conventional scratch test system (WS-2002). In a typical scratch test, a diamond tip of 200 μm was driven through the film surface and gradually loaded to the peak value of 60 N at the rate of 60 N/min with the track length of 4 mm. Subsequently, the scratch morphologies were observed by the optical microscopy (OM) for qualitative and quantitative evaluation.

2.4 Tribological and corrosion testing

Tribo-tests were conducted by using a ball-on-disc tribometer in ambient air and in 3.5 wt% NaCl solution. 5 mm diameter ZrO_2 ceramic balls were used as the counterparts, due to their high hardness, good wear-resistance, chemical inertness and potential applications in water-lubricated components such as bearing and mechanical seals [15]. The applied load was set to 5 N, corresponding to a Hertzian contact pressure of ~ 1.2 GPa. The total time of each test was fixed at 35 min, and the rotation speed and radius were 180 r/min and 4 mm respectively. To assess the repeatability, each test was repeated three times at different locations on the film surface. After tribological tests, the wear tracks and the corresponding counterparts were observed by OM and SEM (SN3400, Hitachi, Japan).

The corrosion resistance of the GLC coated samples was evaluated by using a CHI660E electrochemical setup with a three electrode cell in 3.5 wt% NaCl solution. The working electrode was the coated sample with an active area of 1 cm^2 . The Pt sheet was chosen as the counter electrode, while the reference electrode was an Ag/AgCl electrode. Prior to the test, the samples were immersed in 3.5 wt% NaCl solution for one hour to obtain stable open circuit potentials (OCP). The range of scanning potential for the potentiodynamic polarization curve was set from -1 V to 1.5 V at a scanning rate of 0.5 mV/s. The experiment was repeated twice for each sample. After the tests, the corrosion morphologies were characterized by SEM to analyze the corrosion mechanism.

3. Results and discussion

3.1. Microstructure and composition of GLC films

Surface and cross-sectional morphologies of GLC films with different gradient interlayer thickness are shown in Fig. 1(a-c). Seen from the surface morphologies, the large packs composed of fine particles accumulate on the surface of the films, which grow up gradually and generate more surface defects with the prolonging of the gradient interlayer sputtering time. The cross sections of the three different GLC films show a

dense and uniform columnar morphology with the total thickness of 825 nm, 950 nm, and 1180 nm, respectively. Through-thickness EDX composition scanning shown in Fig. 1(d-f) confirms the tri-layer structure of the films. The Ti adhesive layer shows a distinguishable boundary in the cross-sectional morphologies, corresponding to the highest and stable Ti content in region I (Fig. 1(e)). The Ti-C gradient layer is difficult to distinguish in the SEM images due to the composition gradient in the film structures, but the gradually increasing C content and decreasing Ti content in region II of EDX confirms the presence of Ti-C gradient layer. The top Ti-GLC functional layer is composed of uniform C and Ti elements in region III. In comparison to the other two GLC films, the columnar morphology of GLC-3 is coarser and looser. As the same deposition parameters were used for the Ti adhesive layer and Ti-GLC function layer in all three films, the thickness of these two layers is expected to be similar for all of them, which is approximately 175 nm and 540 nm, respectively, from the cross-sectional SEM and EDX images. The thickness of Ti-C gradient layer can therefore be calculated to increase from about 110 nm to 465 nm as the sputtering time increased from 15 to 60 min.

Fig. 2 shows typical AFM images of the surface topography of the GLC films. Consistent with the SEM results, the surfaces of all of the GLC films are composed of fine and compact granular morphology, which exhibit looser structure and more defects with the increase of gradient interlayer thickness. The surface roughness (R_a) was 3.85 nm, 4.47nm, and 5.52 nm for the GLC-1, GLC-2 and GLC-3 films, respectively.

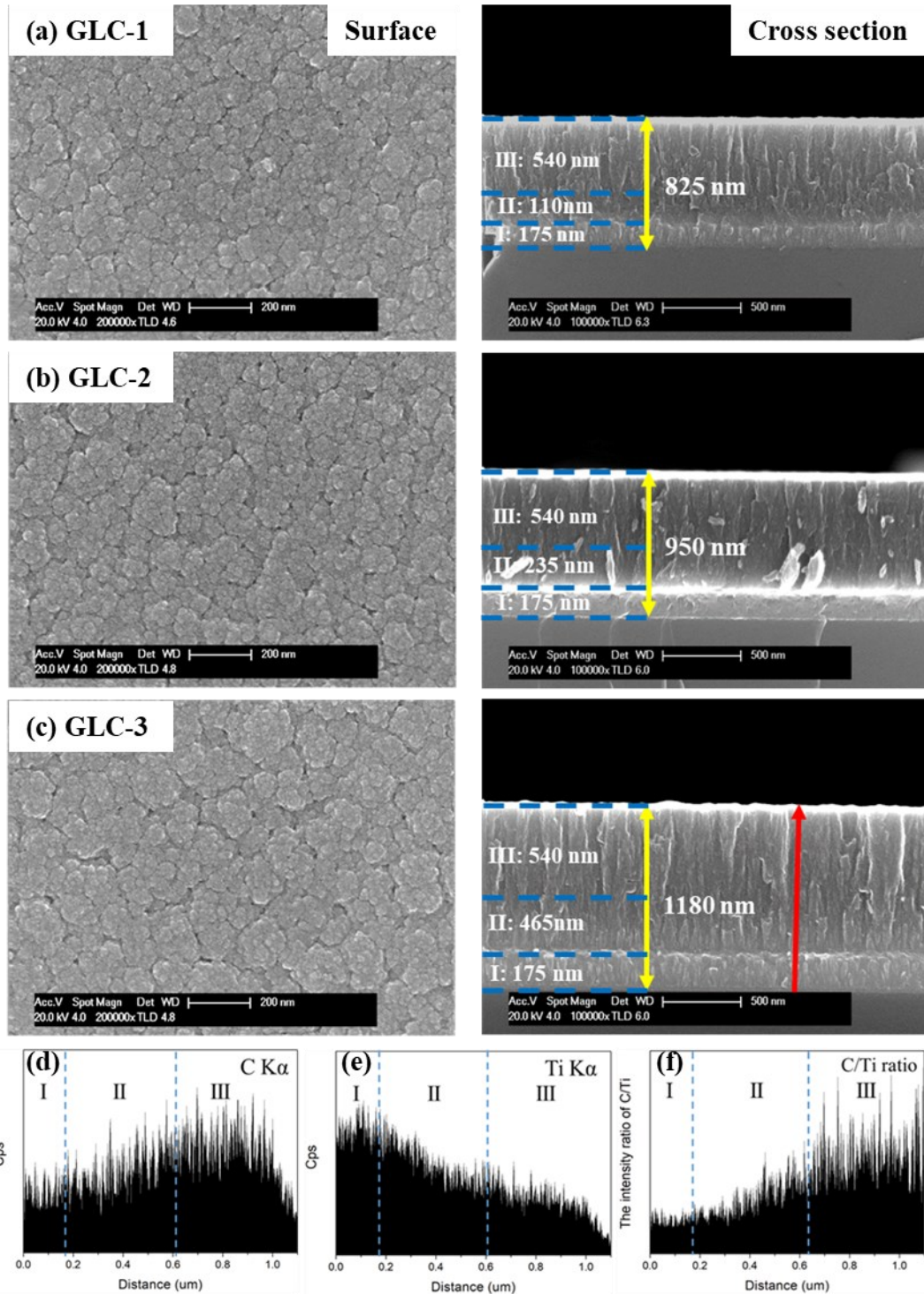


Fig. 1. SEM images of the surface and cross-sectional morphologies of (a) GLC-1, (b) GLC-2, (c) GLC-3, and the typical linear scanning EDX spectra of (d) C element, (e) Ti element and (f) the intensity ratio of C/Ti for GLC-3 (The scanning direction is shown as the red arrow in Fig. 1(c)).

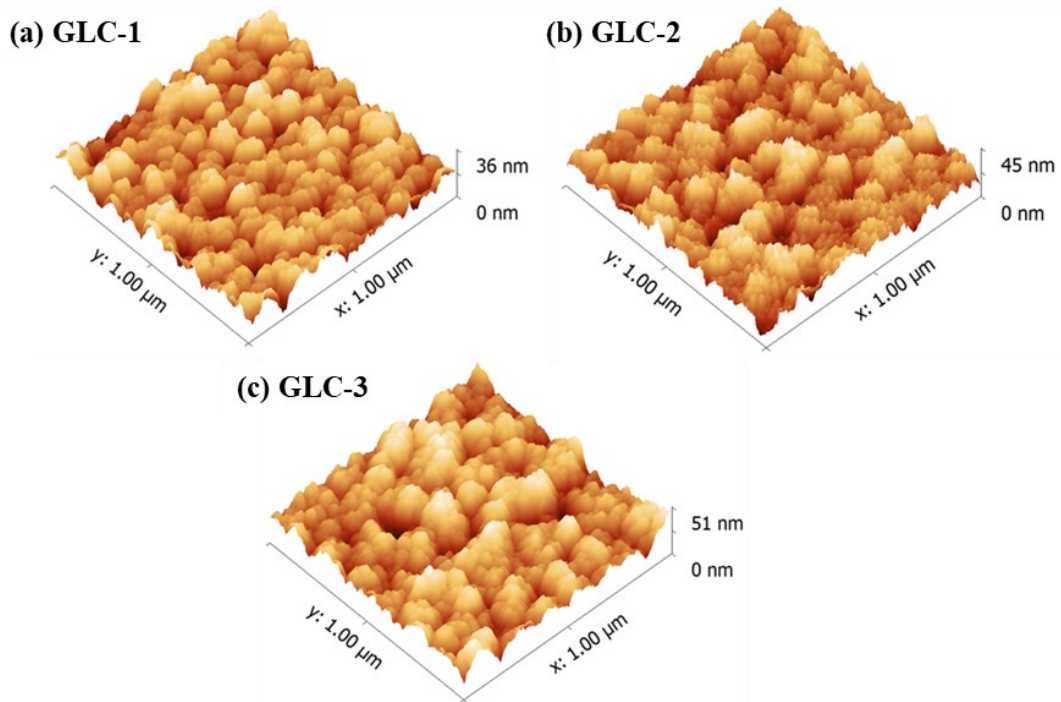


Fig. 2. Typical AFM images of the surface topography of (a) GLC-1, (b) GLC-2, (c) GLC-3.

Gaussian-fitted Raman spectra were used to characterize the variation in carbon atom bonding structure of GLC films with different gradient interlayer thickness, as shown in Fig. 3(a). Two typical characteristic peaks (D peak and G peak) were fitted at approximately 1380 cm^{-1} and 1570 cm^{-1} , respectively, in which the D peak is derived from the breathing modes of sp^2 atoms in clusters of aromatic disorder rings, while the G peak is related to the stretching vibration of all pair of sp^2 atoms in both aromatic rings and olefinic chains [19,22,30]. For more information about the microstructure of GLC films, the area ratio of D peak and G peak (I_D/I_G), the position and the full width at half maximum of the G peak (FWHM) was analyzed as shown in Fig. 3(b). In general, the value of I_D/I_G reflects the size of sp^2 hybridized carbon atoms in the structure, while both the G peak position and the FWHM is related to the disorder of the film structure, resulting from the shape and size distribution of sp^2 cluster, and the distortions of bond length and bond angle, respectively [10,31]. It can be seen that I_D/I_G increases from around 3.35 to about 3.80 with increasing gradient interlayer thickness. Simultaneously, the G peak position at about 1578 cm^{-1} moved to a lower wavelength of approximately 1567 cm^{-1} , and the FWHM increased from 114 cm^{-1} to 134 cm^{-1} . All of the results indicated that the sp^2/sp^3 ratio and the disorder degree of the as-deposited GLC films increase with **increasing gradient interlayer** thickness. Fig. 3(c) shows the XRD patterns of the GLC films, in which the broad diffraction peaks at about $10\text{-}30^\circ$ demonstrated the amorphous structure of the films.

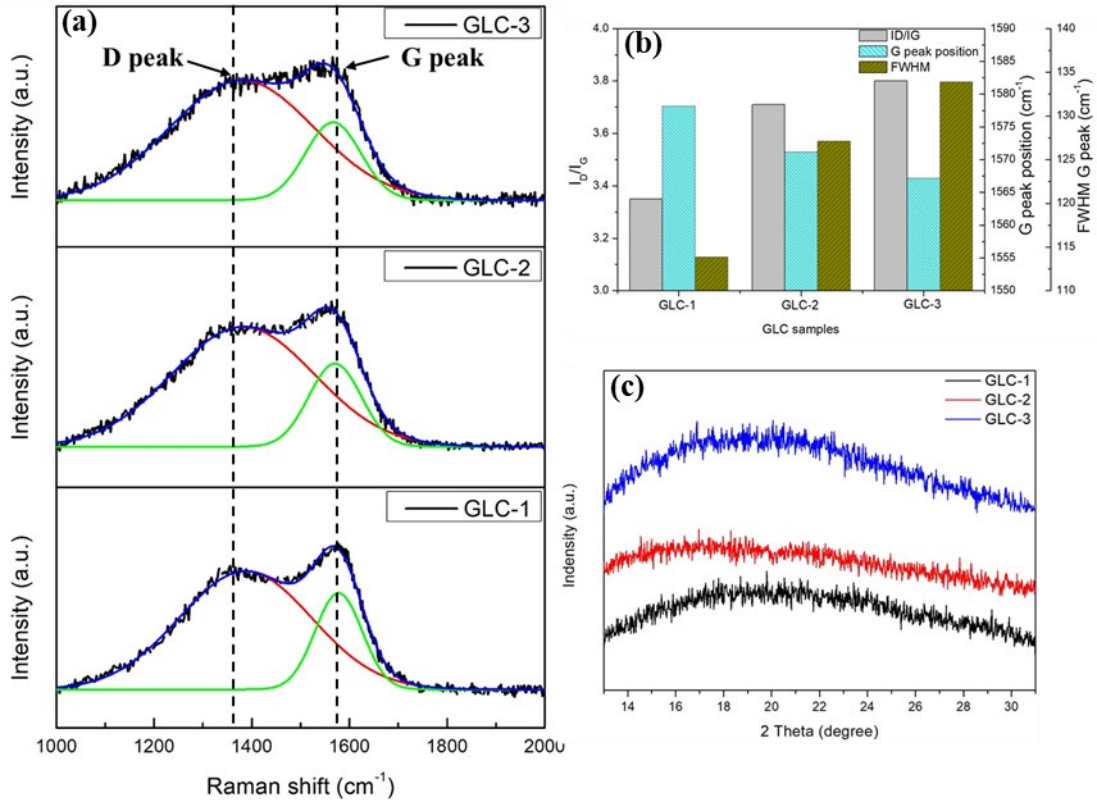


Fig. 3. (a) Raman spectra, (b) I_D/I_G , G peak position and the FWHM of G peak, and (c) XRD patterns of GLC films with different gradient interlayer thickness.

XPS spectra were fitted to determine the chemical bonding structure of the GLC films. As shown in Fig. 4(a-c), the major peak of C 1s can be deconvoluted into five components, which are: (i) C-Ti bond at 282.8 eV, (ii) sp^2 C=C bond at 284.5 eV, (iii) sp^3 C-C bond at 285.2 eV, (iv) C-O bond at 286.5 eV, and (v) C=O bond at 288.5 eV [10,19,32]. A typical Ti 2p XPS spectrum is shown in the insert of Fig. 4(c), which comprises two small peaks located at 459.5 eV (Ti 2p_{3/2}) and 465.2 eV (Ti 2p_{1/2}) which are attributed to the combination of Ti-O and Ti-C bonds. It follows from the above results that the Ti element is doped in the GLC film and reacts with carbon to form titanium carbide in the amorphous carbon structure [19,33,34]. Fig. 4(d) shows the calculated fraction of various carbon bonds of GLC films. It can be seen that the sp^2 hybridized carbon atoms are dominant in the film structure, confirming the graphite-like film structure. The content of sp^2 hybridized bonds increases from about 43.3% to 57.2%, while the fraction of sp^3 hybridized bonds decreases from approximately 36.5% to 26.1% with increasing gradient interlayer thickness. The fraction of C-Ti bonds is around 2.5%, while the carbon-oxygen bonds is in range of to 15-17% as a result of the presence of residual oxygen in the deposition chamber.

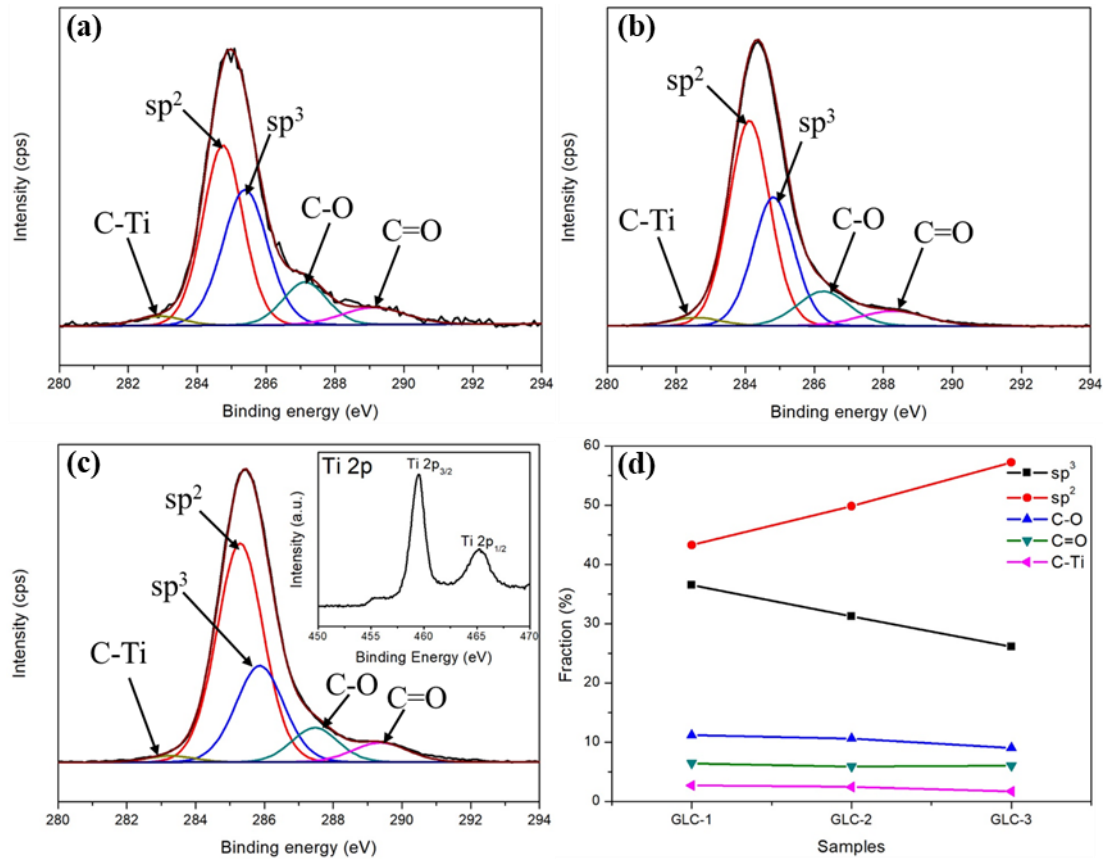


Fig. 4. Fitted C 1s peaks of XPS spectra for (a) GLC-1, (b) GLC-2, (c) GLC-3 (*insert shows a typical XPS spectrum of Ti 2p*), and (d) the fraction of C as sp³, sp², and bonded as C-O, C=O and C-Ti.

Due to the same deposition parameters of the top Ti-GLC function layers, the difference of the microstructure and composition among the GLC films must be closely related to the growth of Ti-C gradient interlayer. Shahsavari et al. [27] reported that the surface roughness of a Cr interlayer could have an important effect on the adsorption and nucleation of DLC films on Si substrate, which increased with the increased thickness of Cr thin film, attributed to the agglomeration of Cr nanoparticles with the increased sputtering time. As the growth template for top GLC film, the columnar structure of Ti-C gradient interlayer may become loose and coarse with increased sputtering time, resulting in more defects and higher surface roughness for GLC films with thicker gradient interlayer. The lower fraction of sp³ carbon atoms for GLC films with thicker gradient interlayer is mainly related to the incorporation of Ti, which can react with C atoms and facilitate the transformation of sp³ bonds to sp² bonds [23,35]. The XPS spectra show that the content of Ti element increases from 2.5% to 4.8% as the gradient interlayer thickness increases from about 110 nm to 465 nm, resulting in the increase of graphitization and disordering of sp² clusters. In addition, the influence of the impinging species energy cannot be completely ignored. Based on the subplantation

model, when the energy of bombarding particles is high enough, the carbonaceous atoms will migrate from the subsurface position towards to the surface, resulting in the decreased density and improved sp^2 carbon content [9,36]. Although the same deposition parameters were used, the extended sputtering time of gradient interlayer causes higher temperature in the SS substrates, which gave rise to the thermalization and relaxation of the subsurface-bound sp^3 carbon. Therefore, the sp^3 fraction decreases with the increased gradient interlayer thickness.

3.2. Mechanical properties of GLC films

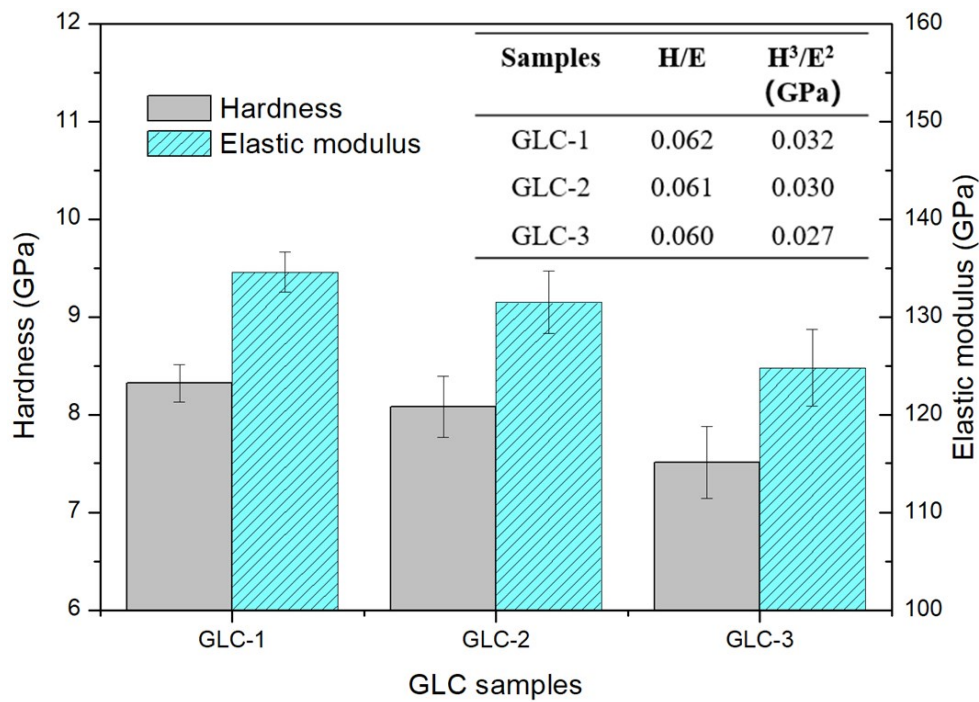


Fig. 5. Hardness (H) and elastic modulus (E) of GLC films with different gradient interlayer thickness (*The insert is the table of H/E and H^3/E^2*).

In general, high hardness of films corresponds to improved wear resistance [13,37]. Fig. 5 shows the hardness and elastic modulus of GLC films with different gradient interlayer thickness. It can be seen that the film hardness (H) decreases from 8.3 GPa to 7.5 GPa as the thickness of gradient interlayer increases from approximately 110 nm to 465 nm. The elastic modulus (E) is 134.6 GPa, 131.5 GPa, and 124.8 GPa for GLC-1, GLC-2 and GLC-3, respectively. As reported in previous studies [10,22,23], the sp^3 bonded carbon atoms play the key role in the hardness of amorphous carbon films, while the sp^2 bonded carbon atoms are largely responsible for their tribological properties. In the GLC films with thinner gradient interlayer, the more sp^3 bonds act as a bridge to improve the interconnection of the adjacent graphite planes, resulting in higher hardness. Besides, the compact microstructure for the GLC-1 film is another

factor for the highest hardness. The ratio of H/E has been reported to be an important indicator of the elastic strain to failure and resilience of hard films, while the value of H^3/E^2 is a measure of the resistance to plastic deformation of hard films [23,38]. Both of these two parameters commonly exhibit positive correlations with the wear resistance. Higher value of H/E and H^3/E^2 (see insert table in Fig. 5) for GLC films with thinner gradient interlayer thickness demonstrated better resilience and improved resistance to plastic deformation, resulting in excellent wear resistance.

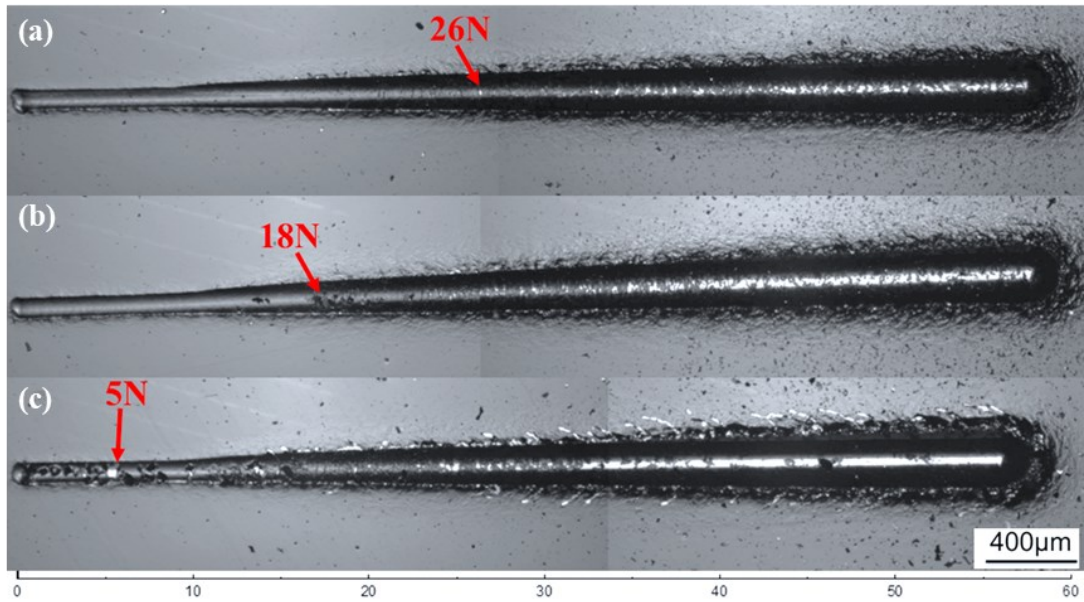


Fig. 6. Optical microscopy images of the scratch track morphologies for (a) GLC-1, (b) GLC-2, (c) GLC-3.

Fig. 6 shows the optical images of the scratch traces for different GLC films. A striking difference in their fracture behavior can be observed depending on the gradient interlayer thickness. Fracture or delamination occurred rapidly for the GLC-3 sample as the progressive normal load was applied, and there was an almost complete stripping for the GLC-3 on the 316L stainless steel at the end of the scratch. The other two GLC films remained intact on the substrates until the applied normal load increased to a critical value (L_c), where the first spallation was detected. As can be seen from Fig. 6, the L_c was 5 N, 18 N, 26 N for GLC-1, GLC-2 and GLC-3, respectively, indicating the scratch adhesion strength between the GLC films and the 316L stainless steel decreases with the increase of gradient interlayer thickness. **This behaviour can be attributed to the high hardness of GLC films with thinner gradient interlayer (Fig. 5), which provided higher load support under progressive loading.** In addition, the higher internal stress of thicker GLC film may also cause its poor bonding strength, as indicated by the wider FWHM of the G peak shown in Fig. 3(b) [31,35].

3.3. Tribological performance of GLC films

3.3.1 Friction and wear properties of GLC films under ambient air and NaCl solution

Fig. 7 (a& b) shows the friction coefficient of the as-deposited GLC films and the uncoated 316L stainless steel substrate (SS) as a function of sliding time at ambient air and 3.5 wt% NaCl solution, respectively. Note that the friction curves are chosen from one group of the three reproducible test results. After a short-term running-in stage the friction coefficient of the substrate increased rapidly to a stable value of about 0.7 in ambient air (Fig. 7(a)). The frictional behavior of the GLC films can be divided into three stages. In the first stage, the friction coefficient decreases dramatically to a steady low value with different durations for GLC films with different gradient interlayer thickness. The friction coefficients for GLC-1, GLC-2 and GLC-3 in stage I were ~ 0.051 , ~ 0.066 and ~ 0.083 , corresponding to sliding durations of ~ 780 s, ~ 300 s and ~ 70 s (Fig. 7(c)), respectively. In other words, the friction coefficient of GLC films increases with increasing gradient interlayer thickness, while the duration of running-in decreases. In stage II, the friction coefficient of GLC films begins to increase, accompanied by a slight fluctuation, and the rate of increase scales with the gradient interlayer thickness. As the sliding process reaches stage III, the friction coefficient has entered a new stable stage, which increases from ~ 0.16 to ~ 0.21 with increasing gradient interlayer thickness.

When sliding in NaCl solution, the friction on the SS substrate followed a similar trend but the stable-state friction coefficient is significantly lower at ~ 0.4 (Fig. 7(b)). Although the friction curves for GLC films also show the three-stage characteristics in NaCl solution, there are some clear differences compared with those in ambient air. During stage I, the friction coefficient of the three GLC samples showed very similar stable values of ~ 0.085 , which is a little higher than those in ambient air. Besides, the duration in this stage shows a huge improvement, particularly for GLC-3, where it increased from ~ 70 s in ambient air to ~ 860 s in NaCl solution (Fig. 7(c)). Furthermore, in comparison to friction sliding in ambient air, no distinct running-in period was observed in the initial stage in NaCl solution. The friction curves in the second stage show more fluctuations, exhibiting a slow upward trend. As in ambient air, the GLC-3 sample reached stage III with a new stable friction coefficient before the others, which were still in the climbing stage at the end of the sliding tests. Interestingly, the final friction coefficient of GLC films in NaCl solution was around 0.4, close to the value of SS substrate. Fig. 7(d) shows the average friction coefficient of GLC films under ambient air and NaCl solution increased with gradient interlayer thickness in both environments.

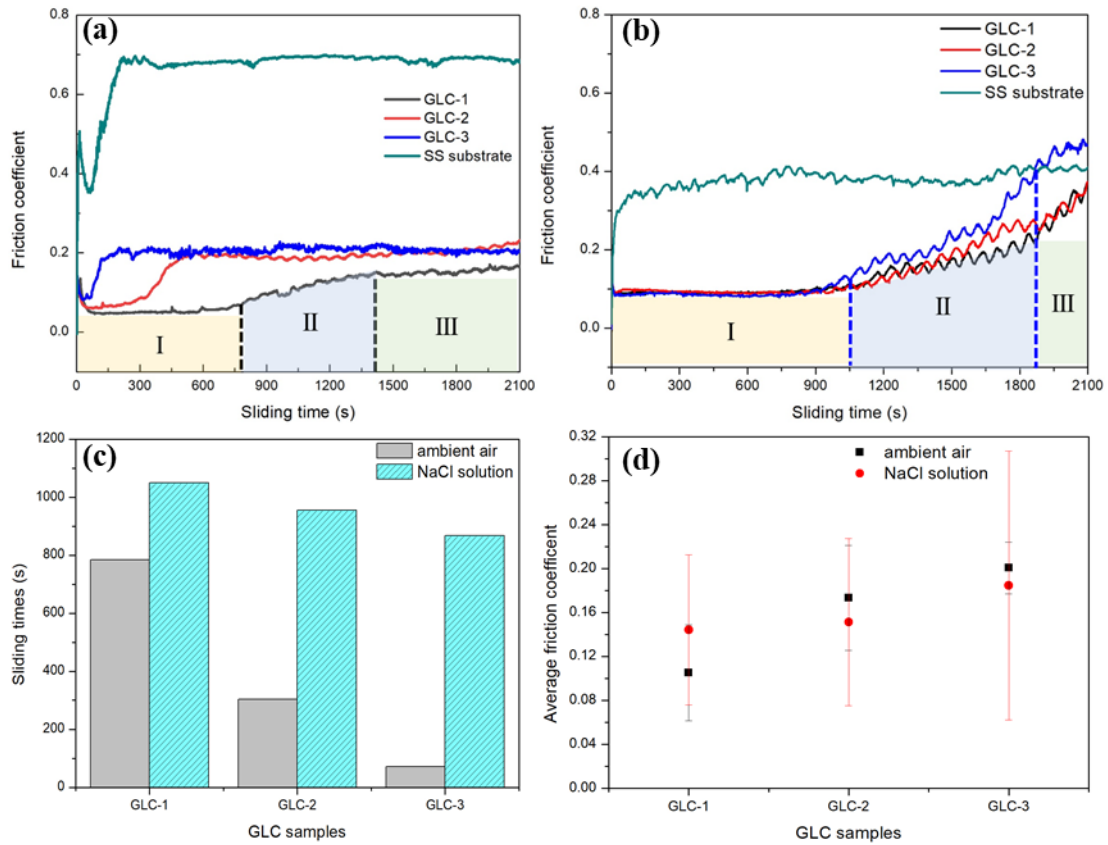


Fig. 7. Friction coefficient as a function of sliding times for GLC films with different gradient interlayer thickness in (a) ambient air, (b) 3.5 w% NaCl solution; (c) the duration of stage I, and (d) the average friction coefficient for GLC films in both ambient air and NaCl solution.

SEM images of the wear tracks in both ambient air and NaCl solution are shown in Fig. 8. When the friction tests are conducted in ambient air, many deep furrows were observed in all of the wear tracks, with some debris at the edge and significant delamination of the films in the centre of the tracks. The width of the wear track increased and the delamination phenomenon became more serious for films with thicker gradient interlayers. For the friction sliding in NaCl solution, the appearance of wear track was totally different from that in ambient air. As can be seen in the images on the right side of Fig.8, the GLC films were completely removed from the surface of the substrate, and track widths were larger than in ambient air. The wear rates were difficult to calculate due to the stripping failure of GLC films.

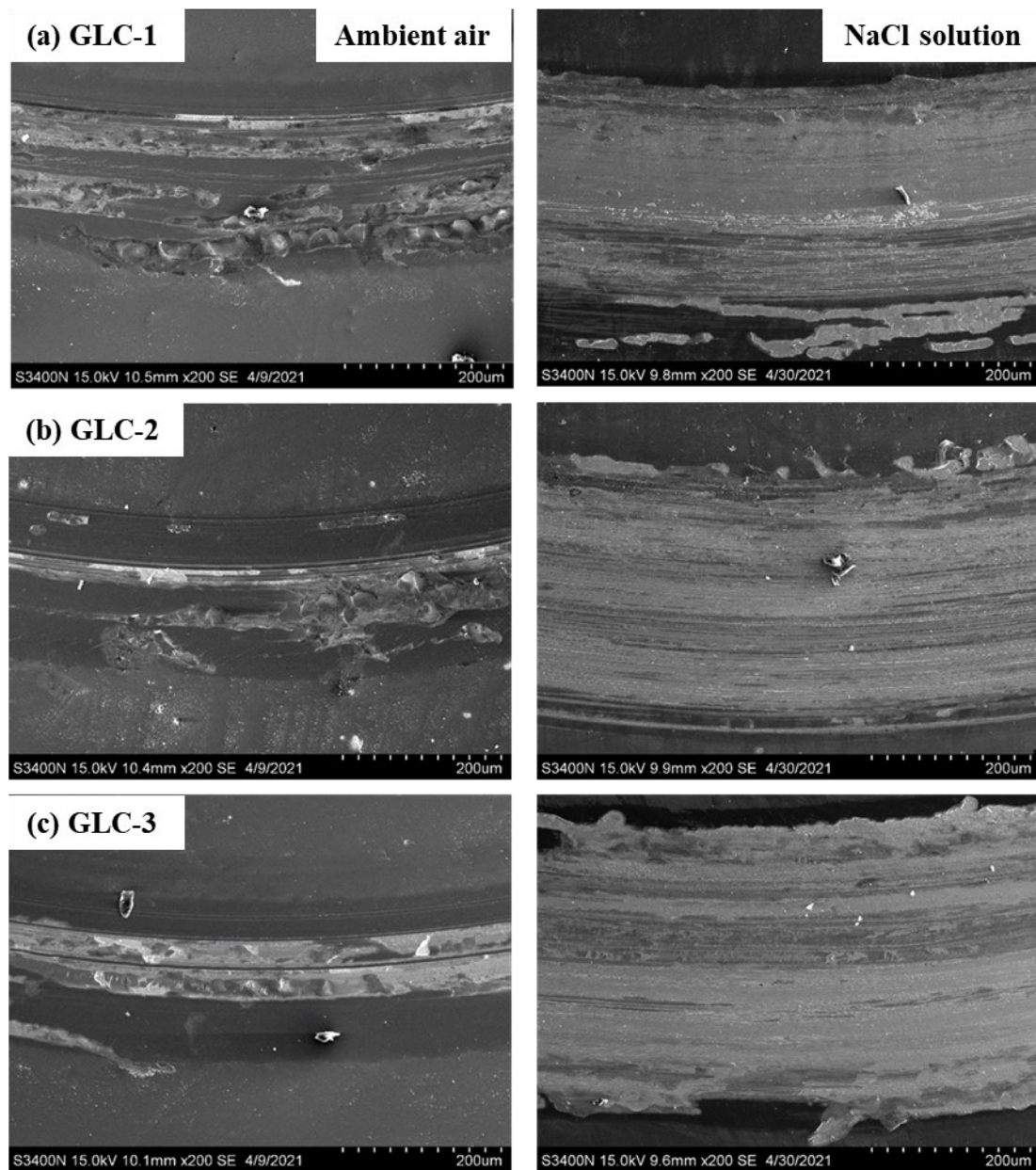


Fig. 8. SEM images of wear track in both ambient air and NaCl solution for (a) GLC-1, (b) GLC-2, (c) GLC-3.

3.3.2 Wear mechanism of GLC films under ambient air and in NaCl solution

In order to understand the wear mechanism of GLC films under different environments, the friction sliding experiments were conducted in ambient air and in NaCl solution in stages I-III. Fig. 9(a-c) shows SEM images of the wear tracks, corresponding EDX maps and optical images of the mating balls at 300 s, 1000 s and 2100 s sliding, corresponding to the three different stages. In ambient air, the wear trace in stage I is smooth with the intact GLC films (Fig. 9(a)). EDX maps also indicated the undamaged film structure. The shallow furrows on the film surface demonstrate abrasion wear in this stage, which has been attributed to the ploughing effect. The small amount of debris

on the mating balls may be ascribed to the formation of graphitized transfer films, which can prevent intimate contact between the films and the ceramic balls and provide the self-lubricating effect for the amorphous films [12,39,40], resulting in the low friction coefficient observed in stage I. **Another reason for the low friction coefficient during stage I can be the phase transformation of hybridized carbon from sp^3 to sp^2 carbon due to the accumulation of friction heating, which has been reported in several previous studies [41-45].** With the increase of abrasive particles in stage I, micro-cracks may form and coalesce caused by the stress concentration, leading to the occurrence of the delamination phenomenon in stage II (Fig. 9(b)). The removal of C and Ti elements and the exposure of Fe element in the EDX maps also confirm the peeling off of the GLC films. The presence of oxygen in the exposed substrate is indicative of tribo-oxidation. These synergistic effects could be the main reasons for the gradually increased friction coefficient during stage II. Furthermore, it can be observed in Fig 9(b&c) that the peeled film in stage II is continuously transferred to the mating balls until the formation of the completed graphitized transfer films in stage III, promoting the stabilisation of the friction coefficient.

As reported previously, the tribological performance of GLC films is correlated with their microstructure, composition and mechanical properties [10,30,46]. Greater sp^2 hybrid bonding in the film structure is generally accepted to be favorable to the formation of carbonaceous transfer-layer on the mated surfaces, reducing the friction coefficient [10,47]. The Raman and XPS results in Fig. (3 &4) demonstrated the graphite-like microstructure in the carbon matrix. However, the friction coefficient of stage I in ambient air increased with increasing gradient interlayer thickness in spite of the increased sp^2 content. One reason for this might be the difference in mechanical properties of the GLC films. The higher H/E , and H^3/E^2 (Fig.5) for the GLC films with thinner gradient interlayer provides more load support to resist the plastic deformation of the film/substrate system, which reduces the real contact area effectively and thus reduces friction. Another factor might be the more compact microstructure and lower surface roughness of the GLC films with thinner gradient interlayer. The dense structure and smooth surface results in less wear particles escaping from the surface and alleviates the abrasive wear. The duration of stage I for GLC films with different gradient interlayer thickness is relevant to the adhesion strength between the film and substrate. The extremely poor bonding strength of GLC-3 shown in Fig.6 leads to its rapid peeling failure as the normal load is applied. Interestingly, the rapid failure of GLC-3 in the first stage is not so detrimental as it may accelerate the formation of graphitized transfer films on the mating balls to achieve the second stable friction

coefficient earlier.

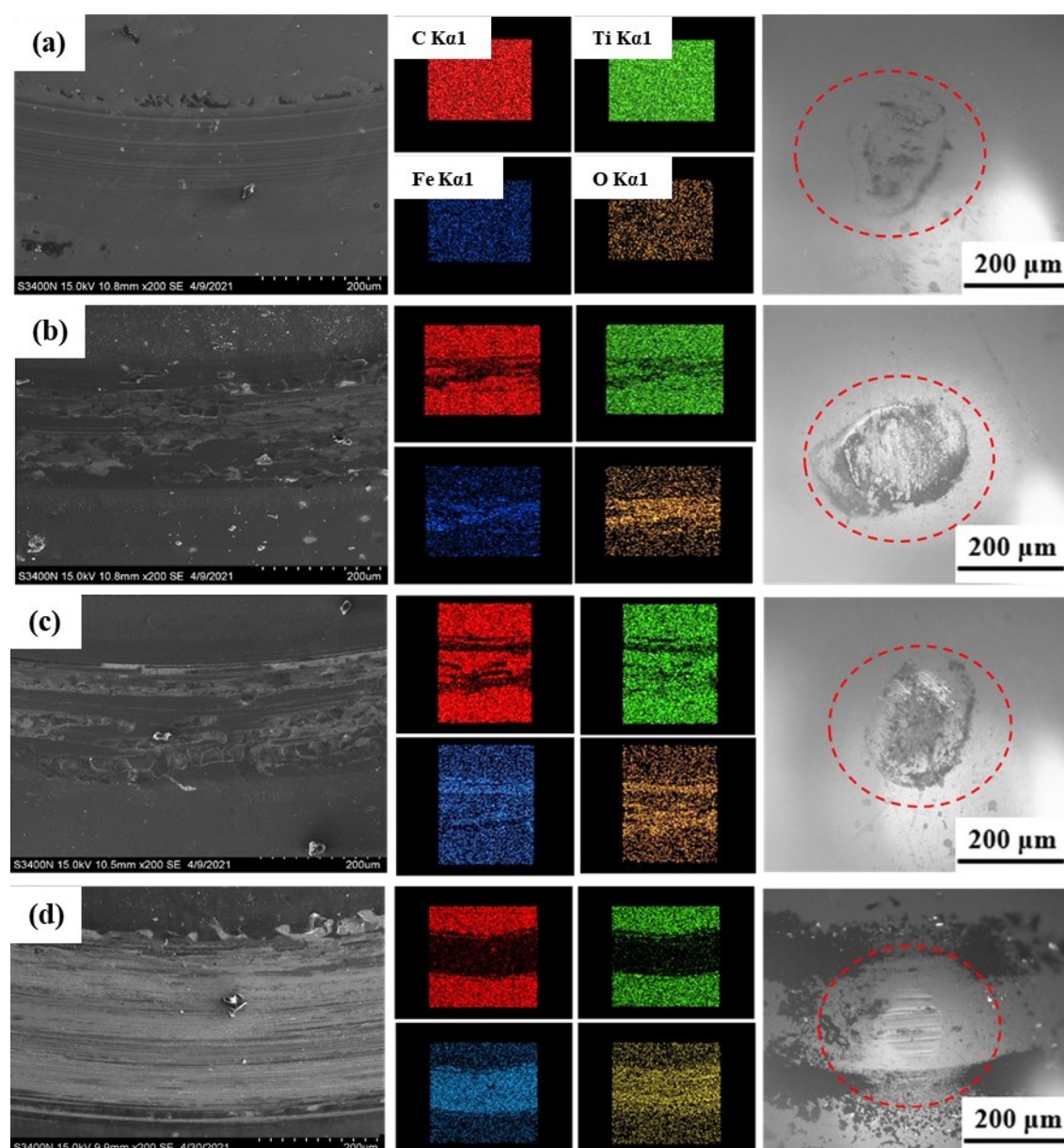


Fig. 9. The SEM images of the wear traces, the corresponding EDX maps and the optical images of the mating balls at (a) 300 s, (b) 1000 s, (c) 2100 s in ambient air for GLC-1 and (d) 2100 s in NaCl solution for GLC-2.

In contrast, under 3.5 wt% NaCl solution, water lubrication causes the lower friction coefficient and very short running-in period observed on the uncoated substrate. All of the GLC films show similar stable and low friction coefficients during stage I, that are a little higher than those in ambient air, in spite of the possible presence of C-H covalent bonds formed by the interaction between the free σ bonds and water molecules at the contact interface [48,49]. The main reason might be the absence of graphitized transfer films on the mating balls as shown in Fig. 9(d). This phenomenon has also been

observed in some previous studies. Zhang et al. found the wear products are difficult to gather on the Al₂O₃ ceramic ball for both hydrogenated and hydrogen free DLC films in pure water environment [50]. Guo et al. [33] also demonstrated the transfer film in the sliding interface was nonexistent when the friction tests with Ti-doped DLC films and GCr15 steel balls friction pairs were conducted in PAO oil lubrication. Wang et al. [47] reported that the friction coefficient for GLC films deposited with different target currents was similar as a result of the similar water lubrication effects at the contact interface, consistent with the similar friction coefficient of GLC films with different gradient interlayers in stage I in our research. The prolonged duration of stage I in NaCl solution might be because the NaCl solution helps eject the hard abrasive particles out from the contact interface during the sliding process. With continued frictional sliding, the NaCl solution will penetrate into the interface of the film/substrate system through the surface defects and micro-pores in the film structure, leading to corrosion of the stainless steel substrate. Therefore, more violent delamination occurred on the film surface in stage II with strong fluctuations of friction coefficient in Fig. 7(b). The more surface defects and decreased film compactness for GLC films with thicker gradient interlayer thickness resulted in faster film failure. In stage III, the film was completely removed and the ZrO₂ balls were in direct contact with the substrate, as confirmed by the EDX maps in Fig. 9(d) and increased coefficient of friction in Fig. 7(b).

3.4. Corrosion properties of GLC films

3.4.1 Polarization curves and corrosion morphologies of GLC films

In order to reveal the effect of gradient interlayer thickness on the corrosion resistance of GLC films, Fig. 10 shows the potentiodynamic polarization curves of the uncoated SS substrate and the GLC films with different gradient interlayer thickness. According to the Tafel fitting of the polarization curves, the corresponding corrosion current density (i_{corr}) and corrosion potential (E_{corr}) for all of the samples are summarized in Table 2. Compared with the uncoated substrate, all of the GLC films show a shift in corrosion potential towards positive values, indicating better corrosion resistance of the GLC films. Especially for the GLC films, the E_{corr} value increases from -0.23 V to -0.19 V since the gradient interlayer thickness decreases from about 465 nm to 110 nm. The value of i_{corr} is generally used to disclose the corrosion rate [19]. As can be seen, the i_{corr} of GLC films is almost one order of magnitude lower than that of the SS substrate (1.78×10^{-6} A/cm²), suggesting effective protection of GLC films against substrate corrosion combined with the diversity of E_{corr} value. For the GLC films, GLC-1 showed the lowest i_{corr} of about 1.72×10^{-7} A/cm², and GLC-3 showed the highest i_{corr} of approximately 5.05×10^{-7} A/cm². E_b and ΔE are also crucial parameters to

evaluate corrosion resistance, with E_b referred to as breakdown or damaging potential and ΔE is the difference between E_b and E_{corr} [17,23]. As shown in Table 2, the E_b and ΔE of GLC-1 and GLC-2 are obviously higher than that of the substrate, implying that the two GLC films can effectively inhibit pitting corrosion on the substrate. Interestingly, the value of E_b and ΔE for GLC-3 is about 0.48 V and 0.71 V, respectively, a little lower than that of the substrate, indicating its poor protecting capability to pitting corrosion.

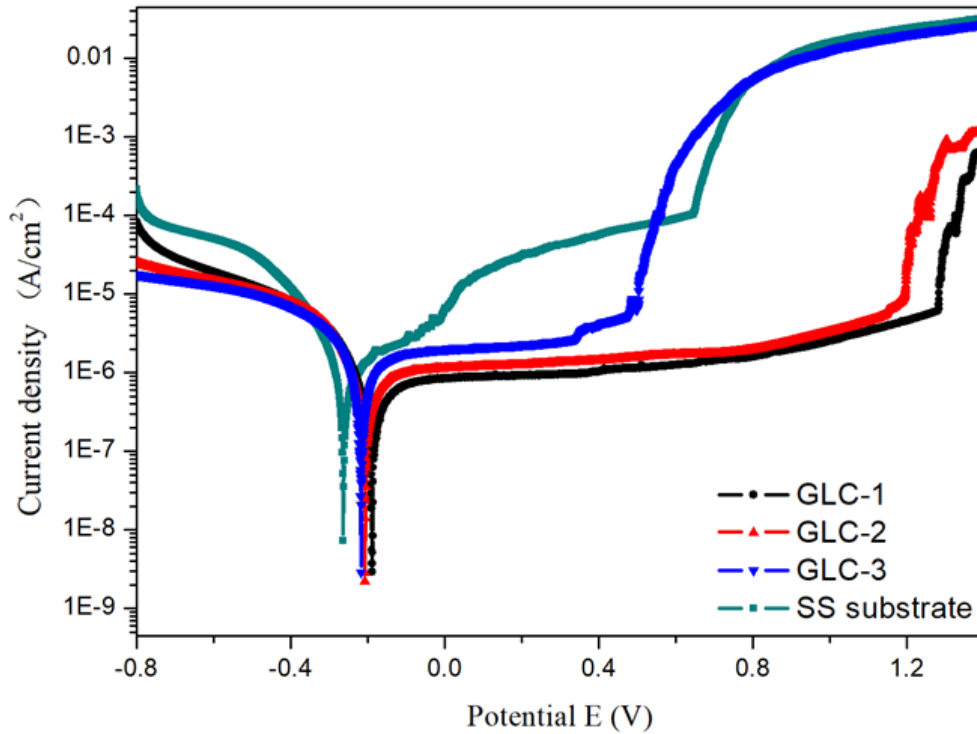


Fig. 10. Potentiodynamic polarization curves of GLC films with different gradient interlayer thickness and the uncoated substrate.

Table 2. Summary of i_{corr} , E_{corr} , E_b , and ΔE values from the fitted potentiodynamic polarization curves.

Samples	316L SS	GLC-1	GLC-2	GLC-3
i_{corr} (A/cm ²)	1.78E-6	1.72E-7	2.91E-7	5.05E-7
E_{corr} (V)	-0.26	-0.19	-0.22	-0.23
E_b (V)	0.64	1.28	1.16	0.48
ΔE (V)	0.9	1.47	1.38	0.71

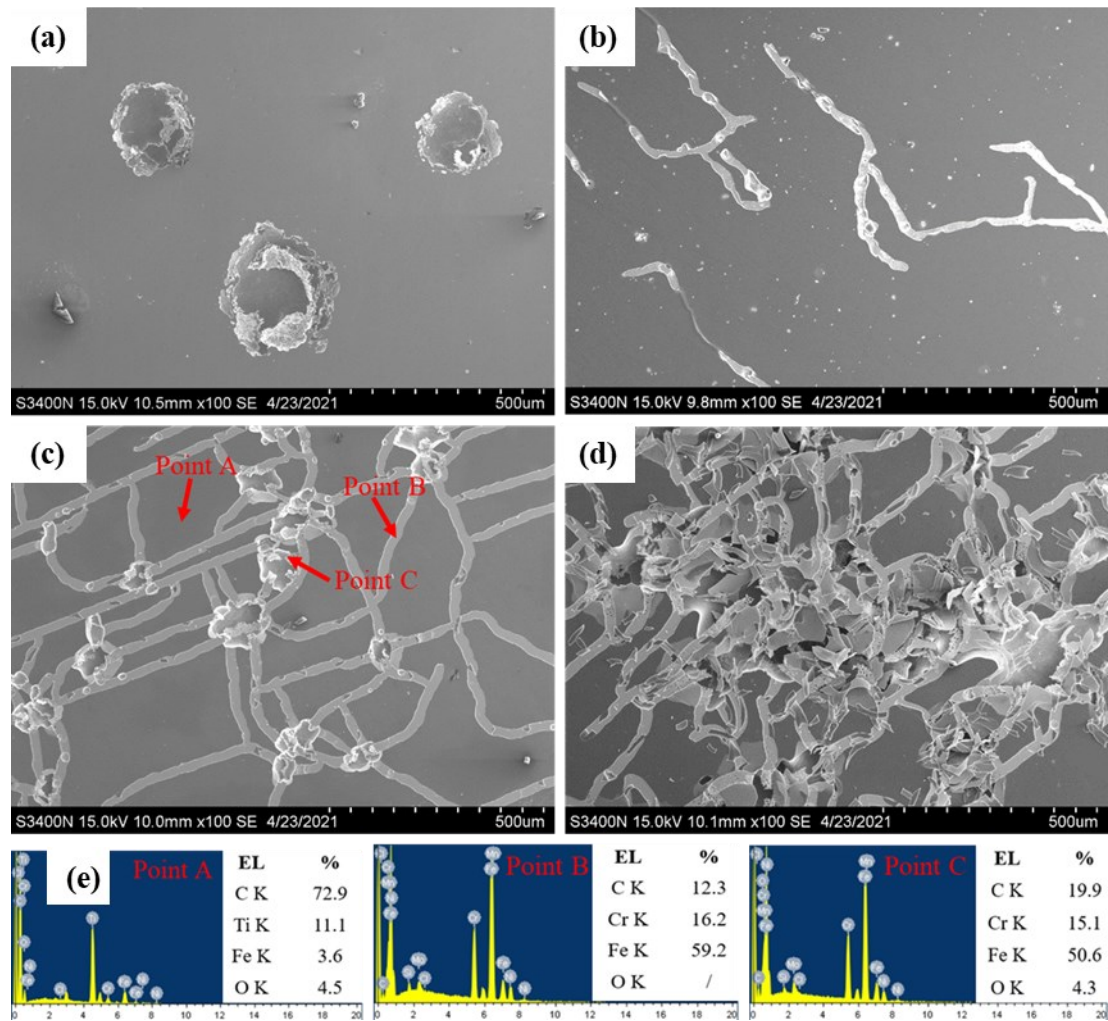


Fig. 11. The corrosion morphologies of the uncoated substrate and the as-deposited GLC films: (a) 316L SS, (b) GLC-1, (c) GLC-2, (d) GLC-3, and (e) EDX spectra for the different points in GLC-2.

Fig. 11(a-d) shows the corrosion morphologies of the uncoated substrate and the as-deposited GLC films with different gradient interlayer thickness. As can be seen, grievous corrosion pits with an average diameter of about 200 μm occurred on the uncoated substrate, which could be attributed to the penetration of Cl^{-1} ions. The corrosion morphologies for all of the GLC films exhibit similar damage characteristics, with strip-like delamination interconnected by many small corrosion pits. Both the size and quantity of the corrosion pits increased with increasing gradient interlayer thickness. The proportion of peeling off area also increased gradually with the gradient interlayer thickness. As shown in Fig. 11(d), only a small amount of film remained attached on the severely corroded surface of GLC-3. The chemical composition at different positions on the surface of GLC-2 was detected by EDX in Fig. 11(e). The composition at point A is dominated by C and Ti elements, indicating the presence of unspooled

carbon films. The oxygen atoms in the film structure may come from residual O₂ in the vacuum chamber. The large amount of Fe element at point B and C demonstrated the removal of GLC films. The presence of O element in the corrosion pits (point C) might be attributed to the formation of iron oxides. Note that almost no oxygen appears in the peeling off area (point B), indicating that corrosion may preferentially occur at film defects.

3.4.2 Corrosion and damage mechanism of GLC films

Defect-free amorphous carbon films have excellent chemical inertness and dense compact structure, which can prevent the penetration of corrosive ions such as chloride ions and oxygen in corrosive environment, thus providing effective protection to the metal substrate. However, some micro-pores and defects are inevitable in the film structure due to the influence of ion bombardment and substrate defects during the deposition process. When the film is exposed to a corrosive medium, it is impossible to completely prevent electrolyte penetrating through the channels formed by these defects and form a destructive effect to the protected active substrate [51]. During the corrosion tests, the corroded substrate will further weaken the adhesion strength between the film and substrate. Then the electrolyte will diffuse along the less adherent interface until to the position of next defect, and finally the pressure of media generates the delamination of the films. Additionally, the accumulated corrosion products at the interface will also promote the peeling off of the GLC films by destroying the weak interface bonding.

Fig. 11, shows that the GLC films with thicker gradient interlayer thickness have peeled off more seriously from the substrates after potentiodynamic polarization tests, which should be firstly attributed to more defects in the films structure and reduced interface bonding between the film and the substrate. The SEM and AFM images (Figs. 1 & 2) show more surface defects on the GLC films with thicker gradient interlayer thickness that will accelerate the penetration of electrolyte to the substrate, and the weak adhesion strength shown in Fig. 6 will provide more channels for the diffusion of electrolyte. The synergistic action of both factors produce the most severe failure for GLC-3 film after the polarization test. The second reason for the difference in corrosion resistance is the change in electrical conductivity of GLC films with different gradient interlayer thickness. Low electrical conductivity will expedite the electron transport over the film surface and thus decrease the corrosion resistance. Reisel et al. [52] claimed that amorphous carbon produces a higher corrosion resistance than crystalline CrN and TiAlN in chloride ion containing electrolytes due to the high electrical resistivity. Bueno et al. [7] found that the high electrical resistivity and excellent bonding strength

promote the H-DLC film to show better corrosion resistance than that of Si-DLC in 3.5 wt% NaCl solution. The Raman and XPS spectra shown in Fig. (2 &3) demonstrate that the GLC films with thicker gradient interlayer thickness have more sp^2 hybridized carbon, signifying higher electrical conductivity and poor corrosion prevention. Furthermore, it was reported that the formation of a galvanic couple between the films and the substrate also has an important effect on the corrosion properties of film/substrate system [7,20,53], inducing and accelerating pitting corrosion. For GLC-3, the high electrical conductivity of GLC films provides channels for electron transport, while surface defects provide ion channels for the electrolyte. Combined with the third condition of potential difference between the GLC film and 316L SS substrate, a galvanic couple will be formed, which could be the main reason for the lower breakdown potential E_b and ΔE of GLC-3 than that of uncoated substrate. When the surface film is essentially completely broken, the current density of GLC-3 is close to that of uncoated substrate shown in Fig.10.

4. Conclusion

Ti-containing multilayer GLC films with different gradient interlayer thickness were deposited on 316L stainless steel by using closed-field unbalanced magnetron sputtering system, and the relationship between microstructure and mechanical properties on their tribological and corrosion behavior was investigated. The sp^2 content and surface roughness increased with increasing gradient interlayer thickness, leading to the lower hardness and adhesion strength combined with the decreased compactness in the film structure. The friction coefficient curves of GLC film in ambient air can be divided into three different stages, corresponding to the abrasive wear, delamination and transfer film formation, respectively. Although similar three stage friction curves were also observed in 3.5% wt NaCl solution, the absence of a transfer film on the mating balls caused the complete failure of GLC films in stage III. Water lubrication effects prolonged the duration in stage I, while Cl^- corrosion accelerated the delamination of GLC films in stage III. The excellent mechanical properties and compact microstructure resulted in better **tribological** properties of GLC films with thinner gradient interlayer thickness in both ambient air and NaCl solution. The improved corrosion potential and decreased corrosion current density indicates the effective protection of GLC films against substrate corrosion, especially for GLC films with thinner gradient interlayer thickness due to the high film compactness and low electrical conductivity. The formation of galvanic couple is likely the main reason for the decreased breakdown potential of GLC-3.

Acknowledgments

The authors gratefully acknowledge the financial support from the Fundamental Research Funds for the Central Universities, China (Grant No: B200201068, B200205011), the Natural Science Foundation of Jiangsu Province of China (BK20210374), the National Natural Science Foundation of China (#11472080) and **the Doctoral Program of Entrepreneurship and Innovation of Jiangsu Province (JSSCBS20210254).**

Declaration of Competing Interest

There are no conflicts to declare.

References:

- [1]K.H. Lo, C.H. Shek, J.K.L. Lai, Recent developments in stainless steels, *Materials Science and Engineering: R: Reports*, 65(2009) 39-104.
- [2]M. Niinomi, Recent metallic materials for biomedical applications, *Metallurgical and Materials Transactions. A, Physical Metallurgy and Materials Science*, 33(2002) 477-486.
- [3]Z. Yu, M. Chen, F. Li, S. Zhu, F. Wang, Synergistic effect of corrosion and wear of the 316 stainless steel in molten zinc alloy at 460 °C, *Corrosion Science*, 165(2020) 108411.
- [4]A. Dalmau, C. Richard, A. Igual Muñoz, Degradation mechanisms in martensitic stainless steels: Wear, corrosion and tribocorrosion appraisal, *Tribology International*, 121(2018) 167-179.
- [5]Y. Ye, Y. Wang, X. Ma, D. Zhang, L. Wang, X. Li, Tribocorrosion behaviors of multilayer PVD DLC coated 304L stainless steel in seawater, *Diamond and Related Materials*, 79(2017) 70-78.
- [6]P.A. Radi, A. Vieira, L. Manfroi, K.C.D.F. Nass, M.A.R. Ramos, P. Leite, G.V. Martins, J.B.F. Jofre, L. Vieira, Tribocorrosion and corrosion behavior of stainless steel coated with DLC films in ethanol with different concentrations of water, *Ceramics International*, 45(2019) 9686-9693.
- [7]A.H.S. Bueno, J. Solis, H. Zhao, C. Wang, T.A. Simões, M. Bryant, A. Neville, Tribocorrosion evaluation of hydrogenated and silicon DLC coatings on carbon steel for use in valves, pistons and pumps in oil and gas industry, *Wear*, 394-395(2018) 60-70.
- [8]K. Bewilogua, D. Hofmann, History of diamond-like carbon films — From first experiments to worldwide applications, *Surface and Coatings Technology*, 242(2014) 214-225.
- [9]J. Robertson, Diamond-like amorphous carbon, *Materials Science & Engineering R Reports*, 37(2002) 129-281.
- [10]D. Dong, B. Jiang, H. Li, Y. Du, C. Yang, Effect of graphite target power density on tribological properties of graphite-like carbon films, *Applied Surface Science*, 439(2018) 900-909.
- [11]D. Du, D. Liu, Z. Ye, X. Zhang, F. Li, Z. Zhou, L. Yu, Fretting wear and fretting fatigue behaviors of diamond-like carbon and graphite-like carbon films deposited on Ti-6Al-4V alloy, *Applied Surface Science*, 313(2014) 462-469.
- [12]S.K. Field, M. Jarratt, D.G. Teer, Tribological properties of graphite-like and diamond-like carbon coatings, *Tribology International*, 37(2004) 949-956.
- [13]M. Yan, X. Wang, S. Zhang, S. Zhang, X. Sui, W. Li, J. Hao, W. Liu, Friction and wear properties of GLC and DLC coatings under ionic liquid lubrication, *Tribology International*, 143(2020) 106067.

- [14]Y. Wang, L. Wang, J. Li, J. Chen, Q. Xue, Tribological properties of graphite-like carbon coatings coupling with different metals in ambient air and water, *Tribology International*, 60(2013) 147-155.
- [15]Y. Wang, J. Li, L. Wang, J. Chen, Q. Xue, Tribological Performances of Graphite-Like Carbon Films Coupled to Different Ceramics in Ambient Air and Water, *Tribology International*, 56(2013) 333-341.
- [16]K. Wang, H. Zhou, K. Zhang, X. Liu, X. Feng, Y. Zhang, G. Chen, Y. Zheng, Effects of Ti interlayer on adhesion property of DLC films: A first principle study, *Diamond and Related Materials*, 111(2021).
- [17]T. Borowski, K. Kulikowski, B. Adamczyk-Cieślak, K. Roźniatowski, M. Szychalski, M. Tarnowski, Influence of nitrided and nitrocarburised layers on the functional properties of nitrogen-doped soft carbon-based coatings deposited on 316L steel under DC glow-discharge conditions, *Surface and Coatings Technology*, 392(2020) 125705.
- [18]D. Liu, T. Yang, H. Ma, Y. Liang, The microstructure, bio-tribological properties, and biocompatibility of titanium surfaces with graded zirconium incorporation in amorphous carbon bioceramic composite films, *Surface and Coatings Technology*, 385(2020) 125391.
- [19]X. Xu, Y. Zhou, L. Liu, P. Guo, X. Li, K. Lee, P. Cui, A. Wang, Corrosion behavior of diamond-like carbon film induced by Al/Ti co-doping, *Applied Surface Science*, 509(2020) 144877.
- [20]H.A. Esquivel-Puentes, T.S. Fisher, G. Capote, J.J. Olaya, Bias effects on wear and corrosion behavior of amorphous hydrogenated carbon films with zirconia interlayer, *Surface and Coatings Technology*, 350(2018) 603-620.
- [21]S. Nissen, J. Heeg, M. Warkentin, D. Behrend, M. Wienecke, The effect of deposition parameters on structure, mechanical and adhesion properties of a-C:H on Ti6Al4V with gradient Ti-a-C:H:Ti interlayer, *Surface and Coatings Technology*, 316(2017) 180-189.
- [22]Y. Wang, J. Pu, J. Wang, J. Li, J. Chen, Q. Xue, Interlayer design for the graphite-like carbon film with high load-bearing capacity under sliding-friction condition in water, *Applied Surface Science*, 311(2014) 816-824.
- [23]S. Zhang, M. Yan, Y. Yang, Y. Zhang, F. Yan, H. Li, Excellent mechanical, tribological and anti-corrosive performance of novel Ti-DLC nanocomposite thin films prepared via magnetron sputtering method, *Carbon*, 151(2019) 136-147.
- [24]B. Zhou, Z. Liu, B. Tang, A.V. Rogachev, Catalytic effect of Al and AlN interlayer on the growth and properties of containing carbon films, *Applied Surface Science*, 326(2015) 174-180.
- [25]W. Yu, J. Wang, W. Huang, L. Cui, L. Wang, Improving high temperature tribological performances of Si doped diamond-like carbon by using W interlayer, *Tribology International*, 146(2020) 106241.
- [26]H. Zhu, L. Ma, N. Liu, Q. Wei, D. Wu, Y. Wang, H. Long, Z. Yu, Improvement in anti-corrosion property of hydrogenated diamond-like carbon film by modifying CrC interlayer, *Diamond and Related Materials*, 72(2017) 99-107.
- [27]F. Shahsavari, M. Ehteshamzadeh, M.R. Naimi-Jamal, A. Irannejad, Nanoindentation and nanoscratch behaviors of DLC films growth on different thickness of Cr nanolayers, *Diamond and Related Materials*, 70(2016) 76-82.
- [28]Q. Chen, C. Zeng, M. Xu, H. Yuan, H. Lv, Z. Wang, X. Wang, Effect of SiN₃ interlayer thickness on adhesion and friction properties of diamond-like carbon films, *Diamond and Related Materials*, 94(2019) 186-193.
- [29]W.S. Hincapie C., J.M. Gutiérrez B., V.J. Trava-Airoldi, J.J. Olaya F., J.E. Alfonso, G. Capote, Influence of the TixSi and TixSi/a-Si:H interlayers on adherence of diamond-like carbon coatings,

Diamond and Related Materials, 109(2020) 108079.

- [30]X. Sui, J. Liu, S. Zhang, J. Yang, J. Hao, Microstructure, mechanical and tribological characterization of CrN/DLC/Cr-DLC multilayer coating with improved adhesive wear resistance, Applied Surface Science, 439(2018) 24-32.
- [31]A.C. Ferrari, J. Robertson, Interpretation of Raman spectra of disordered and amorphous carbon, Physical Review B, 61(2000) 14095-14107.
- [32]J.B. Cai, X.L. Wang, W.Q. Bai, X.Y. Zhao, T.Q. Wang, J.P. Tu, Bias-graded deposition and tribological properties of Ti-contained a-C gradient composite film on Ti6Al4V alloy, Applied Surface Science, 279(2013) 450-457.
- [33]Y. Guo, P. Guo, L. Sun, X. Li, P. Ke, Q. Li, A. Wang, Tribological properties of Ti-doped diamond-like carbon coatings under dry friction and PAO oil lubrication, Surface and Interface Analysis, 51(2019) 361-370.
- [34]C. Kong, P. Guo, L. Sun, Y. Zhou, Y. Liang, X. Li, P. Ke, K. Lee, A. Wang, Tribological mechanism of diamond-like carbon films induced by Ti/Al co-doping, Surface and Coatings Technology, 342(2018) 167-177.
- [35]B. Zhou, Z. Liu, A.V. Rogachev, D.G. Piliptsov, B. Tang, Size effect in the titanium/diamond-like carbon bilayer films: effect of relative thickness on their structure and mechanical properties, Surface and Interface Analysis, 49(2017) 47-54.
- [36]H.Y. Dai, X.R. Cheng, C.F. Wang, Y.C. Xue, Z.P. Chen, Structural, optical and electrical properties of amorphous carbon films deposited by pulsed unbalanced magnetron sputtering, Optik, 126(2015) 861-864.
- [37]C.A. Charitidis, Nanomechanical and nanotribological properties of carbon-based thin films: A review, International Journal of Refractory Metals and Hard Materials, 28(2010) 51-70.
- [38]J. Musil, F. Kunc, H. Zeman, H. Poláková, Relationships between hardness, Young's modulus and elastic recovery in hard nanocomposite coatings, Surface and Coatings Technology, 154(2002) 304-313.
- [39]Y.L. Gong, P.P. Jing, Y.J. Zhou, D.L. Ma, Q.Y. Deng, R. Shen, N. Huang, Y.X. Leng, Formation of rod-shaped wear debris and the graphitization tendency of Cu-doped hydrogenated diamond-like carbon films, Diamond and Related Materials, 102(2020) 107654.
- [40]P. Xu, X. Cao, M. Zhang, W. Yue, G. Zhang, Friction and wear behaviors of different DLC films sliding against SiC and Si₃N₄ balls under high relative humidity, Diamond and Related Materials, 108(2020) 107977.
- [41]Y. Liu, L. Chen, B. Zhang, Z. Cao, P. Shi, Y. Peng, N. Zhou, J. Zhang, L. Qian, Key role of transfer layer in load dependence of friction on hydrogenated diamond-like carbon films in humid air and vacuum, Materials, 12(2019) 1550.
- [42]Y. Liu, B. Yu, Z. Cao, P. Shi, N. Zhou, B. Zhang, J. Zhang, L. Qian, Probing superlubricity stability of hydrogenated diamond-like carbon film by varying sliding velocity, Applied Surface Science, 439(2018) 976-982.
- [43]T.F. Zhang, F. Jiang, T.T. Liao, Q.Y. Deng, S.S. Li, Y. Wang, Y.X. Leng, Tribological behavior of diamond like carbon film sliding against CoCrMo or Al₂O₃ in air and water environment, Tribology International, 95(2016) 456-461.
- [44]K. Ohara, N.A.B. Masripan, N. Umehara, H. Kousaka, T. Tokoroyama, S. Inami, K. Zushi, M. Fujita, Evaluation of the transformed layer of DLC coatings after sliding in oil using spectroscopic reflectometry, Tribology International, 65(2013) 270-277.

- [45]T.W. Scharf, I.L. Singer, Role of the Transfer Film on the Friction and Wear of Metal Carbide Reinforced Amorphous Carbon Coatings During Run-in, *Tribology International*, 36(2009) 43-53.
- [46]X. Shi, T.W. Liskiewicz, B.D. Beake, J. Chen, C. Wang, Tribological performance of graphite-like carbon films with varied thickness, *Tribology International*, 149(2020) 105586.
- [47]Y. Wang, J. Li, L. Shan, J. Chen, Q. Xue, Tribological performances of the graphite-like carbon films deposited with different target powers in ambient air and distilled water, *Tribology International*, 73(2014) 17-24.
- [48]H. Ronkainen, S. Varjus, K. Holmberg, Tribological performance of different DLC coatings in water-lubricated conditions, *Wear*, 249(2001) 267-271.
- [49]H. Ronkainen, S. Varjus, J. Koskinen, K. Holmberg, Differentiating the tribological performance of hydrogenated and hydrogen-free DLC coatings, *Wear*, 249(2001) 260-266.
- [50]T.F. Zhang, D. Xie, N. Huang, Y. Leng, The effect of hydrogen on the tribological behavior of diamond like carbon (DLC) coatings sliding against Al₂O₃ in water environment, *Surface and Coatings Technology*, 320(2017) 619-623.
- [51]G. Wu, L. Sun, W. Dai, L. Song, A. Wang, Influence of interlayers on corrosion resistance of diamond-like carbon coating on magnesium alloy, *Surface and Coatings Technology*, 204(2010) 2193-2196.
- [52]G. Reisel, G. Irmer, B. Wielage, A. Dorner-Reisel, Electrochemical corrosion behavior of carbon-based thin films in chloride ions containing electrolytes, *Thin Solid Films*, 515(2006) 1038-1042.
- [53]Z.M. Wang, J. Zhang, X. Han, Q.F. Li, Z.L. Wang, R. Wei, Corrosion and salt scale resistance of multilayered diamond-like carbon film in CO₂ saturated solutions, *Corrosion Science*, 86(2014) 261-267.